



Full Length Article

Quantification of the resonant energy transfer processes in $\text{Er}^{3+}/\text{Yb}^{3+}$ co-doped $\text{Ca}_3\text{Al}_2\text{Si}_3\text{O}_{12}$ glassesEugenio Cantelar^{a,*}, Ginés Lifante^a, Lorena Grima^b, José Ignacio Peña^b, Daniel Sola^{c,d}^a Dpto. de Física de Materiales, C-04, Facultad de Ciencias, Universidad Autónoma de Madrid, 28049-Madrid, Spain^b Instituto de Nanociencia y Materiales de Aragón, Universidad de Zaragoza-CSIC, 50018-Zaragoza, Spain^c Laboratorio de Óptica, Centro de Investigación en Óptica y Nanofísica, Universidad de Murcia, 30100-Murcia, Spain^d Aragonesa Foundation for Research and Development (ARAD), Government of Aragon, 50018-Zaragoza, Spain

ARTICLE INFO

Keywords:

 $\text{Er}^{3+}/\text{Yb}^{3+}$

Energy transfer

Calcium aluminosilicate

Concentration dependence

ABSTRACT

The resonant cross relaxation processes between Yb^{3+} and Er^{3+} ions in calcium aluminosilicate glasses have been quantified under selective Er^{3+} excitation. The infrared emission spectra, measured under steady state conditions (CW excitation to the $^4\text{I}_{9/2}$ erbium level), have allowed to obtain an experimental relationship linking the transfer ($\text{Yb}^{3+} \rightarrow \text{Er}^{3+}$) and back transfer ($\text{Er}^{3+} \rightarrow \text{Yb}^{3+}$) parameters. These measurements combined with the dynamics of the main emitting levels, measured under pulsed excitation to the $^2\text{H}_{11/2}$ erbium level, have allowed the fully quantification of the energy transfer parameters. The obtained values, $C_{25} = 5.5 \times 10^{-18} \text{ cm}^3 \text{ s}^{-1}$ ($\text{Yb}^{3+} \rightarrow \text{Er}^{3+}$), $C_{52} = 1.5 \times 10^{-18} \text{ cm}^3 \text{ s}^{-1}$ ($\text{Er}^{3+} \rightarrow \text{Yb}^{3+}$) and $C_{27} = 7.6 \times 10^{-18} \text{ cm}^3 \text{ s}^{-1}$ (up-conversion mechanism, estimated from the Judd-Ofelt analysis previously reported), can be used to predict the temporal evolution of the main luminescent emission bands.

1. Introduction

Throughout the last decades, lanthanide activated crystalline materials and glasses have attracted great attention because of their potential applications in different scientific and technological fields such as lighting [1], solar cells [2], photonics [3] and biomedicine [4].

Among the trivalent lanthanide ions, Er^{3+} ions have played an important role in the development of solid state lasers and amplifiers because of their intense and efficient emission band ($^4\text{I}_{13/2} \rightarrow ^4\text{I}_{15/2}$ transition) in the eye-safe $1.5 \mu\text{m}$ spectral region. The main drawback that presents this active ion is its low absorption cross section in the infrared, which limits the final device pump efficiency.

The material sensitization with Yb^{3+} ions has been widely explored [5–8] and it is considered nowadays the best option to overcome the low pumping efficiency of Er^{3+} -doped materials [9]. First, they provide an intense absorption band, $^2\text{F}_{7/2} \rightarrow ^2\text{F}_{5/2}$, covering a broad infrared spectral range ($900 \text{ nm} \leq \lambda \leq 1020 \text{ nm}$), where this transition partially overlaps with the $^4\text{I}_{15/2} \rightarrow ^4\text{I}_{11/2}$ erbium absorption band ($970 \text{ nm} \leq \lambda \leq 1000 \text{ nm}$). The second reason is the energetic coincidence of both excited levels, $^2\text{F}_{5/2}$ (Yb^{3+}) and $^4\text{I}_{11/2}$ (Er^{3+}), which is responsible for the apparition of resonant energy transfer mechanisms between Er^{3+} and

Yb^{3+} ions. The study and characterization of energy transfer mechanisms between Yb^{3+} and Er^{3+} ions have played a fundamental role in the development of a large number of optimized lasers in which the energy transfer leads to an efficient excitation of Er^{3+} ions [10–17].

Calcium aluminosilicate glasses ($\text{Ca}_3\text{Al}_2\text{Si}_3\text{O}_{12}$) are interesting candidates to be used in photonic applications that demands the use of lanthanide activated materials, as they present excellent mechanical and thermal properties in addition to a wide transparent range, high refractive index and good corrosion resistance [18]. In comparison with other glasses, the maximum phonon energy of $\text{Ca}_3\text{Al}_2\text{Si}_3\text{O}_{12}$ is lower ($\hbar\omega_{\text{max}} \sim 1050 \text{ cm}^{-1}$) than those observed, for instance, in phosphates or borates ($\hbar\omega_{\text{max}} \sim 1300 - 1350 \text{ cm}^{-1}$) [19–21]. Thus, lower values for the non-radiative transition probabilities are expected in $\text{Ca}_3\text{Al}_2\text{Si}_3\text{O}_{12}$ and, therefore, the radiative decays of trivalent lanthanide ions in this glass can achieve higher luminescence quantum efficiencies than in phosphate or borate glasses.

In this work, the resonant cross relaxation processes between Yb^{3+} and Er^{3+} ions in $\text{Ca}_3\text{Al}_2\text{Si}_3\text{O}_{12}$ glasses are quantified under selective Er^{3+} excitation. A continuous wave (CW) pumping scheme at $\lambda_{\text{exc}} \sim 0.8 \mu\text{m}$, matching $^4\text{I}_{15/2} \rightarrow ^4\text{I}_{9/2}$ Er^{3+} absorption band, has been used to obtain a relationship between the macroscopic energy parameters from $\text{Yb}^{3+} \rightarrow$

* Corresponding author. Avda. Francisco Tomás y Valiente n° 7 Departamento de Física de Materiales, C-04 Facultad de Ciencias Universidad Autónoma de Madrid 28049 – MADRID (Spain)

E-mail address: eugenio.cantelar@uam.es (E. Cantelar).

<https://doi.org/10.1016/j.jlumin.2022.119484>

Received 18 July 2022; Received in revised form 27 October 2022; Accepted 30 October 2022

Available online 5 November 2022

0022-2313/© 2023 Published by Elsevier B.V. This is an open access article under the CC BY-NC-ND license (<http://creativecommons.org/licenses/by-nc-nd/4.0/>).

Table 1Er³⁺ and Yb³⁺ concentrations in the glasses studied in the present work.

Sample	Er ³⁺ (wt%)	Yb ³⁺ (wt%)
# 0	0	0.5
# 1	0.5	0
# 2	0.5	0.1
# 3	0.5	0.5
# 4	0.5	1.0
# 5	0.5	2.0

Er³⁺ and from Er³⁺ → Yb³⁺, commonly known as transfer and back transfer parameters. On the other hand, the dynamics of the main emitting levels as function of Yb³⁺ concentration has been investigated under pulsed excitation at $\lambda_{exc} \sim 532$ nm, matching the $^4I_{15/2} \rightarrow ^2H_{11/2}$ erbium absorption band. These measurements, combined with a model based on the rate equations formalism, have allowed the full quantification of the energy transfer parameters. The obtained values have a general validity as they are independent on the excitation scheme used for their evaluation. Therefore, their knowledge is an essential tool that will allow the design of future photonic devices such as infrared to visible energy converters, optical amplifiers and lasers based on Er³⁺/Yb³⁺ co-doped calcium aluminosilicate glasses.

2. Experimental procedure

Yb³⁺ and Er³⁺ singly doped and Er³⁺/Yb³⁺ co-doped Ca₃Al₂Si₃O₁₂ glasses have been fabricated from precursor rods obtained by mixing the adequate quantities of CaO (Aldrich, 99.9%), Al₂O₃ (Sigma-Aldrich, 99.99%) and SiO₂ (Aldrich, 99.6%) powders. The trivalent lanthanide ions, Er³⁺ and/or Yb³⁺, were added to the composites as Er₂O₃ and/or Yb₂O₃ (both from Aldrich, 99.9%) to obtain the desired single or co-doped samples. In all cases, the composites have been isostatically pressed at 200 MPa during 3 min to obtain ceramic rods that were sintered at 1200 °C during 12 h. Glass samples were manufactured by means of the Laser Floating Zone (LFZ) technique. Description of this laser technique can be found elsewhere [22–24]. This fabrication procedure provides both high axial and radial cooling gradients to manufacture glass samples. Specifically, glass samples were obtained at a growth rate of 500 mm/h. The lanthanide concentrations in the fabricated glasses are summarized in Table 1.

The spectroscopic characterization has been performed by using CW and pulsed excitations schemes: a Millennia pumped Ti:Sapphire laser has been used to study the infrared luminescent bands under steady state conditions while the second harmonic of a pulsed Nd:YAG laser (Spectra Physics model DCR 2/2 A 3378) was required to explore the temporal behaviour of the dominant emission bands (VIS and IR). Regardless on the excitation scheme, the luminescence signal was dispersed through an ARC monochromator (SpectraPro 500-i) and then detected by a Thorn EMI photomultiplier (QB9558) or a Judson InGaAs photodiode, depending on the spectral region (visible or infrared, respectively). Additionally, in measurements under pulsed excitation, a Tektronix DPO4104B-L digital oscilloscope was used to average and record the temporal evolution of the luminescent signals.

3. Results and discussion

3.1. Steady-state conditions: ratio between the macroscopic transfer parameters

The fine structure splitting associated to the fundamental electronic configuration of Er³⁺ ions ($[Xe]4f^{11}$), $^{2S+1}L_J$ energy levels, offer a wide variety of excitation schemes when they are embedded in a solid.

In the particular case of Er³⁺/Yb³⁺ co-doped samples, among the different $^{2S+1}L_J$ erbium levels, the CW excitation to the $^4I_{9/2}$ manifold ($\lambda \sim 0.8$ μ m) has been proved to be appropriate for establishing an

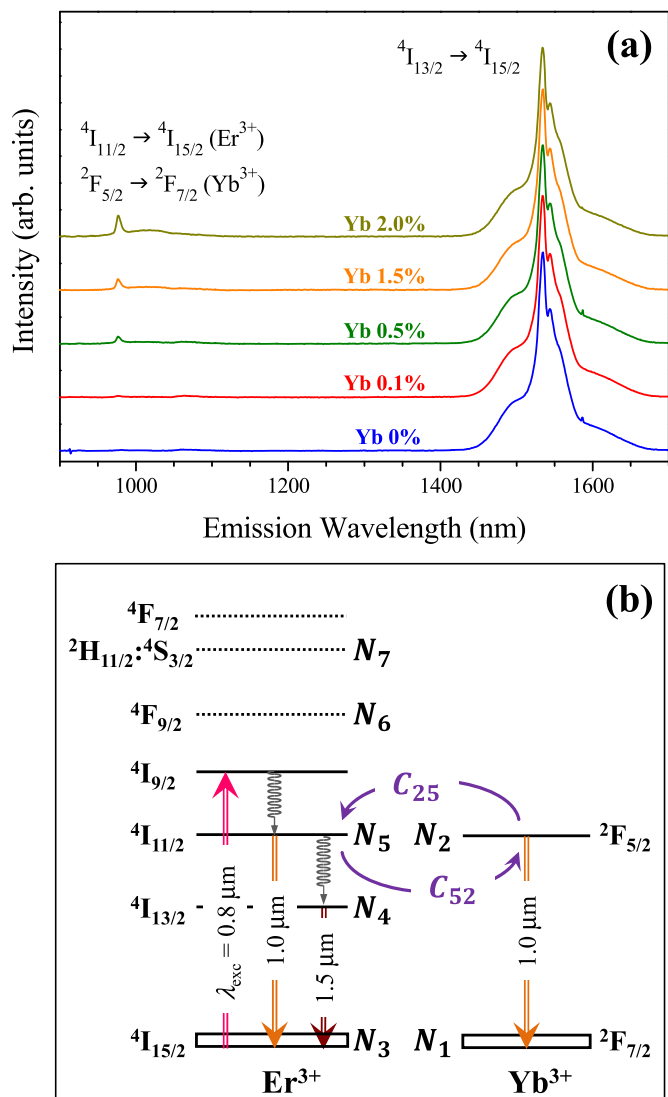


Fig. 1. (a) Emission spectra under CW excitation at 0.8 μ m ($^4I_{15/2} \rightarrow ^4I_{9/2}$ Er³⁺ absorption band) measured in samples #1 to #5. (b) Partial energy level diagram showing the dominant emission bands and the cross-relaxation processes between Er³⁺ and Yb³⁺ ions.

empirical expression relating the macroscopic parameters that characterize the cross relaxation mechanisms between both ions; that is, the transfer from Yb³⁺ to Er³⁺ and the back transfer from Er³⁺ to Yb³⁺ [8].

Additionally, at sufficiently low pump powers, the excitation through the $^4I_{15/2} \rightarrow ^4I_{9/2}$ absorption band presents the additional advantage that it minimizes the infrared to visible up-conversion processes, and therefore, under these conditions, the population induced in the erbium upper levels can be neglected. This fact facilitates the task of obtaining a relationship which links the transfer and back transfer parameters, as it will be seen later.

Fig. 1(a) shows the emission spectra in the 900–1700 nm spectral range measured under CW excitation at $\lambda_{exc} = 0.8$ μ m in Er³⁺/Yb³⁺ co-doped Ca₃Al₂Si₃O₁₂ glasses with fixed erbium concentration ([Er³⁺] = 0.5 wt%) and variable ytterbium content ([Yb³⁺] = 0, 0.1, 0.5, 1.0 and 2.0 wt%, samples #1 - #5). As it can be appreciated, independently on the Yb³⁺ concentration, the spectra are dominated by the characteristic emission band of erbium ions at around $\lambda_{emi} \sim 1.5$ μ m, although a second band, much weaker, can also be detected at around $\lambda_{emi} \sim 1.0$ μ m.

As it is indicated in Fig. 1(b), considering the small energy gap between $^4I_{9/2}$ and $^4I_{11/2}$ erbium levels ($\Delta E \sim 2160$ cm⁻¹) [25], the relaxation from the $^4I_{9/2}$ level efficiently populates the $^4I_{11/2}$ manifold

via multiphonon relaxation. In Er^{3+} singly doped samples, the decay from this level is partially radiative to the ground state giving rise to the $^4\text{I}_{11/2} \rightarrow ^4\text{I}_{15/2}$ emission band ($\lambda_{\text{emi}} \sim 1.0 \mu\text{m}$) and partially non-radiative to the lower lying level $^4\text{I}_{13/2}$, from where the relaxation is basically radiative to the ground state, $^4\text{I}_{13/2} \rightarrow ^4\text{I}_{15/2}$ transition ($\lambda_{\text{emi}} \sim 1.5 \mu\text{m}$).

Additionally, in $\text{Er}^{3+}/\text{Yb}^{3+}$ co-doped samples, the energetic coincidence of $^4\text{I}_{11/2}$ (Er^{3+}) and $^2\text{F}_{5/2}$ (Yb^{3+}) manifolds makes possible that the $^4\text{I}_{11/2}$ level relaxes to the ground state by transferring the excitation to Yb^{3+} ions across the resonant cross-relaxation process $^4\text{I}_{11/2} \rightarrow ^4\text{I}_{15/2}$ (Er^{3+}): $^2\text{F}_{7/2} \rightarrow ^2\text{F}_{5/2}$ (Yb^{3+}). This mechanism is commonly known as back transfer process [5–9] and, as it is indicated in Fig. 1(b), it will be characterized by a macroscopic transfer parameter C_{52} .

The decay from the excited ytterbium level is basically governed by the radiative transition $^2\text{F}_{5/2} \rightarrow ^2\text{F}_{7/2}$ and the transfer to Er^{3+} ions through the opposite cross relaxation process $^2\text{F}_{5/2} \rightarrow ^2\text{F}_{7/2}$ (Yb^{3+}): $^4\text{I}_{15/2} \rightarrow ^4\text{I}_{11/2}$ (Er^{3+}), transfer process characterized by the C_{25} parameter. The conjunction of both processes, radiative decay and transfer to Er^{3+} ions, gives rise to a net increment of the emission band intensity located at around $\lambda_{\text{emi}} = 1.0 \mu\text{m}$. A detailed inspection of Fig. 1(a) reveals that this fact is particularly appreciable in samples with high Yb^{3+} content, $[\text{Yb}^{3+}] > 0.5 \text{ wt\%}$ (samples #3 to #5). The line shape of this emission band corresponds to the spectral overlap between the $^4\text{I}_{11/2} \rightarrow ^4\text{I}_{15/2}$ and $^2\text{F}_{5/2} \rightarrow ^2\text{F}_{7/2}$ of erbium and ytterbium transitions, respectively. Therefore, the weight of each transition in the emission line shape is determined by the ratio between the population of the corresponding erbium and ytterbium excited states. Taking into account that both levels are linked by cross relaxation mechanisms, the excitation of one of them gives rise to a transient state that evolves until transfer ($\text{Yb}^{3+} \rightarrow \text{Er}^{3+}$) and back transfer ($\text{Er}^{3+} \rightarrow \text{Yb}^{3+}$) processes are balanced. This is automatically translated to a dynamical equilibrium between the population densities in the $^4\text{I}_{11/2}$ (Er^{3+}) and $^2\text{F}_{5/2}$ (Yb^{3+}) multiplets. As will be shown below, the presence of this dynamical equilibrium allows the determination of both transfer and back transfer parameters, C_{25} and C_{52} respectively.

As it has been previously mentioned, at sufficiently low pump powers, the excitation at $0.8 \mu\text{m}$ produces a negligible population of the erbium upper levels (up-conversion levels) but also a negligible depletion of the ground state of both ions. Under these conditions, the population dynamics of the infrared levels (see Fig. 1(b)) can be described by the following rate equations:

$$\frac{dN_5}{dt} = R_p N_3 + C_{25} N_2 N_3 - C_{52} N_5 N_1 - A_{5m} N_5 \quad (1)$$

$$\frac{dN_4}{dt} = (A_{54} + W_{54}^{\text{NR}}) N_5 - A_{4m} N_4 \quad (2)$$

$$\frac{dN_2}{dt} = C_{52} N_5 N_1 - C_{25} N_2 N_3 - A_{2m} N_2 \quad (3)$$

$$N_3 = N_{\text{Er}} - N_4 - N_5 \approx N_{\text{Er}} \quad (4)$$

$$N_1 = N_{\text{Yb}} - N_2 \approx N_{\text{Yb}} \quad (5)$$

where R_p (in s^{-1}) is the pumping rate, N_i ($i = 1, 2, \dots, 5$) represents the population density of i -th level (in cm^{-3}), N_{Er} and N_{Yb} symbolize the total Er^{3+} and Yb^{3+} concentrations (in cm^{-3}), A_{ij} and W_{ij}^{NR} (in s^{-1}) are the radiative and non-radiative transition probabilities associated to the $i \rightarrow j$ transition, and A_{im} is the total transition probability that can be evaluated from the experimental lifetime value (τ_i) as $A_{im} = 1/\tau_i$ (see Table 4).

Under steady state conditions ($dN_i/dt = 0$) eqs. (3)–(5) imply that:

$$0 \approx C_{52} N_5 N_{\text{Yb}} - C_{25} N_2 N_{\text{Er}} - A_{2m} N_2 \quad (6)$$

and, therefore, the population ratio in the dynamical equilibrium is given by:

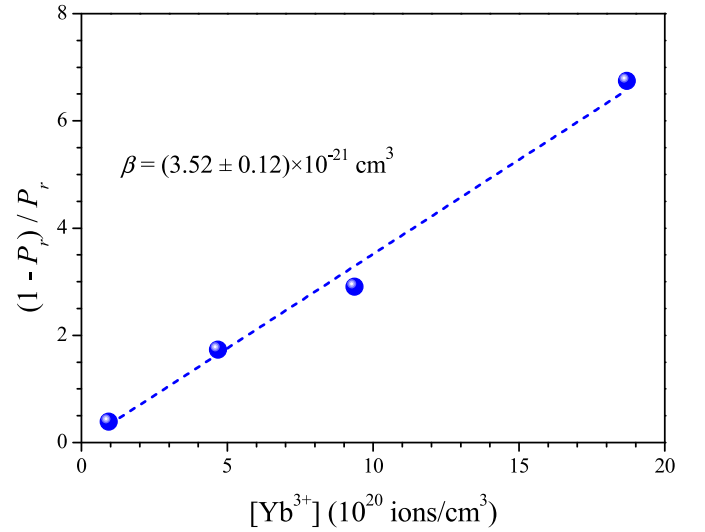


Fig. 2. Experimental values of $(1 - P_r)/P_r$ as function of Yb^{3+} concentration, and least squares fit to eq. (9), solid symbols and dashed line respectively.

$$\frac{N_2}{N_5} \approx \frac{C_{52} N_{\text{Yb}}}{C_{25} N_{\text{Er}} + A_{2m}} \quad (7)$$

Last expression indicates that under steady state conditions, the ratio between the population densities of the resonant levels reach a value that depends on the total Er^{3+} and Yb^{3+} concentrations, the macroscopic transfer (C_{25}) and back-transfer (C_{52}) parameters and the total transition probability of the ytterbium excited state (A_{2m}).

In order to experimentally determine the dynamical equilibrium, N_2/N_5 value, a magnitude P_r is often defined as the ratio between the $^4\text{I}_{11/2} \rightarrow ^4\text{I}_{15/2}$ erbium emission (P_{53}) over the total emission at $1.0 \mu\text{m}$ in co-doped samples ($P_{53} + P_{21}$) [5]:

$$P_r = \frac{P_{53}}{P_{53} + P_{21}} \quad (8)$$

where P_{ij} can be determined from the emission spectrum as the area of the $i \rightarrow j$ emission band ($P_{ij} \propto \int I_{ij}(\lambda) d\lambda$). Taking into account the energy gap between the $^2\text{F}_{5/2}$ and $^2\text{F}_{7/2}$ ytterbium levels ($\Delta E \sim 10,000 \text{ cm}^{-1}$) and the gap law reported for $\text{Ca}_3\text{Al}_2\text{Si}_3\text{O}_{12}$ glasses [25], it can be assumed that the multiphonon processes can be neglected in the relaxation of Yb^{3+} ions; thus, $A_{2m} = A_{21} + W_{21}^{\text{NR}} \approx A_{21}$. Under these conditions, eq. (8) can be conveniently rewritten as:

$$\frac{1 - P_r}{P_r} = \frac{A_{2m}}{A_{53}} \frac{C_{52}}{C_{25} N_{\text{Er}} + A_{2m}} N_{\text{Yb}} \quad (9)$$

Thus, in $\text{Er}^{3+}/\text{Yb}^{3+}$ co-doped samples with fixed Er^{3+} concentration and variable Yb^{3+} concentration, the magnitude $(1 - P_r)/P_r$ should present a linear relation with Yb^{3+} concentration, being the slope value (β):

$$\beta = \frac{A_{2m}}{A_{53}} \frac{C_{52}}{C_{25} N_{\text{Er}} + A_{2m}} \quad (10)$$

From the experimental point of view, in co-coped samples, it is impossible to determine P_{53} and P_{21} in an isolated way since the corresponding transitions appear spectrally overlapped. In order to overcome such problem, the overall $\text{Er}^{3+}/\text{Yb}^{3+}$ emission at around $1.0 \mu\text{m}$ ($P_{53} + P_{21}$) is compared with the Er^{3+} emission at $1.5 \mu\text{m}$ (P_{43} , $^4\text{I}_{13/2} \rightarrow ^4\text{I}_{15/2}$ transition), which ratio with the $^4\text{I}_{11/2} \rightarrow ^4\text{I}_{15/2}$ emission can be determined in Er^{3+} singly doped samples [5,7,8]:

$$P_r = \frac{P_{43}}{P_{53} + P_{21}} \left[\frac{P'_{53}}{P'_{43}} \right] \quad (11)$$

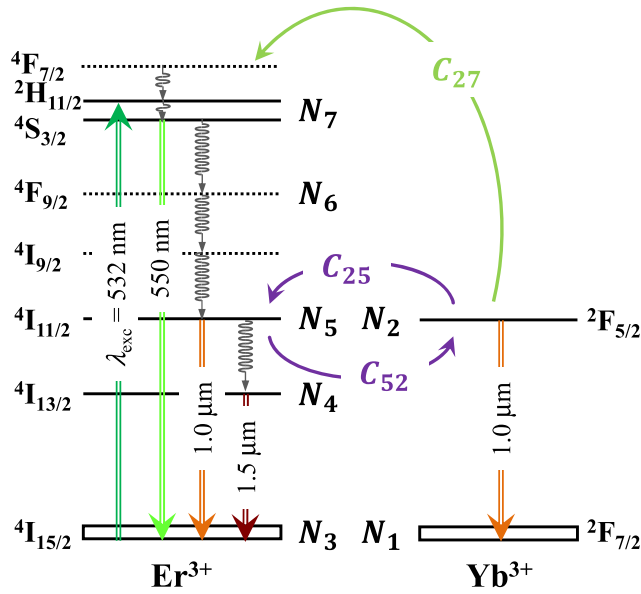


Fig. 3. Partial energy level diagram showing the main emissions under pulsed excitation at $\lambda_{\text{exc}} = 532$ nm. The different transfer processes between Er^{3+} and Yb^{3+} ions have been also included.

where P'_{53}/P'_{43} represents the ratio between $4I_{11/2} \rightarrow 4I_{15/2}$ and $4I_{13/2} \rightarrow 4I_{15/2}$ emission bands in the erbium singly doped sample.

Following eq. (11), the emission spectra shown in Fig. 1(a) were integrated to calculate the area under the 1.0 μm and 1.5 μm emission bands in order to obtain the P_r values. The experimental values (dots) of the magnitude $(1 - P_r)/P_r$ as function of Yb^{3+} concentration, together with the least squares fit to eq. (9) (dashed line), are presented in Fig. 2.

As it can be observed, the experimental $(1 - P_r)/P_r$ values increase monotonously with the Yb^{3+} concentration, and this dependency can be quite well described by the linear trend previously deduced, eq. (9). The slope value, $\beta = (3.52 \pm 0.12) \times 10^{-21} \text{ cm}^3$, links the transfer and back transfer parameters establishing the following empirical relationship between them:

$$C_{52} = \frac{A_{53}}{A_{2m}} \beta (C_{25} N_{\text{Er}} + A_{2m}) \quad (11)$$

Last expression, together with the information obtained from the population dynamics under pulsed excitation (next section), allow the modelling of the energy transfer processes between both ions and, by comparing with the experimental data, the fully determination of the transfer parameters as it will be shown in section 3.3.

3.2. Population dynamics under pulsed excitation

The population dynamics in samples #1 to #5 was investigated under pulsed excitation by using the second harmonic of a Nd:YAG laser ($\lambda_{\text{exc}} = 532$ nm). As it is sketched in Fig. 3, this excitation wavelength matches the $4I_{15/2} \rightarrow 2H_{11/2}$ erbium absorption. The radiative and non-radiative relaxations from the $2H_{11/2}$ level populate the main emitting manifolds. In fact, as indicated in that figure, three emission bands can be detected under this excitation scheme: a visible emission corresponding to the radiative decay from the thermally coupled manifolds $2H_{11/2} \rightarrow 4S_{3/2}$ to the ground state ($\lambda_{\text{emi}} \sim 550$ nm), the radiative decay from the resonant levels $4I_{11/2}$ (Er^{3+}) and $2F_{5/2}$ (Yb^{3+}) to their ground states ($\lambda_{\text{emi}} \sim 1.0$ μm) and the characteristic emission of Er^{3+} ions, $4I_{13/2} \rightarrow 4I_{15/2}$ transition ($\lambda_{\text{emi}} \sim 1.5$ μm).

Under pulsed excitation at $\lambda_{\text{exc}} = 532$ nm, the luminescence temporal evolution associated to the erbium transitions $2H_{11/2} \rightarrow 4S_{3/2} \rightarrow 4I_{15/2}$ and $4I_{13/2} \rightarrow 4I_{15/2}$ exhibits a single exponential decay even at high Yb^{3+}

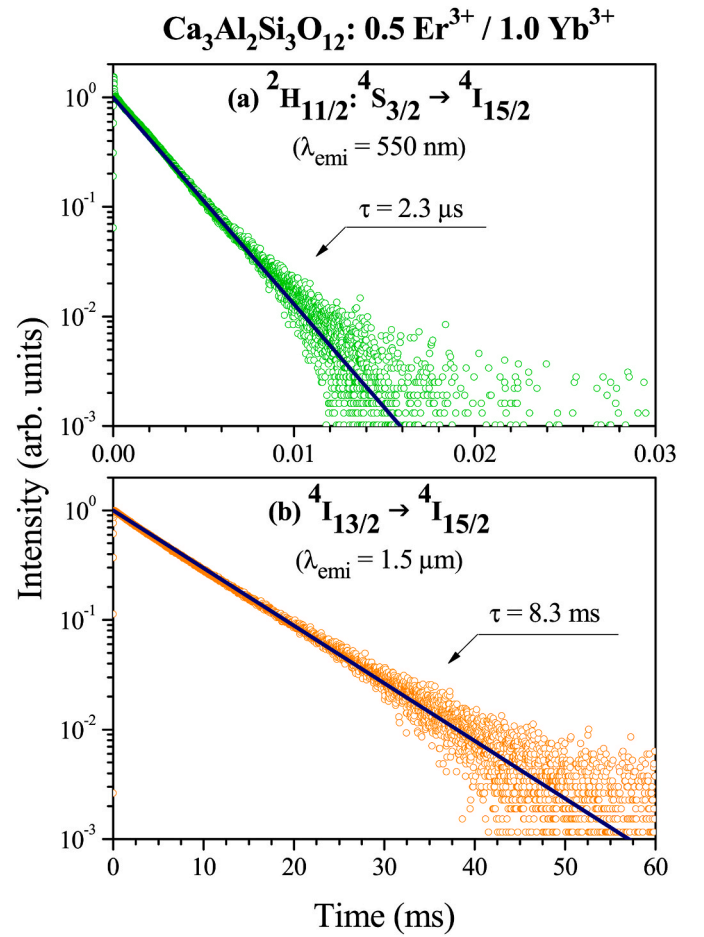


Fig. 4. Temporal evolution of the luminescence corresponding to (a) $2H_{11/2} \rightarrow 4S_{3/2} \rightarrow 4I_{15/2}$ and (b) $4I_{13/2} \rightarrow 4I_{15/2}$ Er^{3+} transitions measured under pulsed excitation at $\lambda_{\text{exc}} = 532$ nm.

Table 2

Lifetime values of $2H_{11/2} \rightarrow 4S_{3/2}$ and $4I_{13/2}$ erbium manifolds as function of Yb^{3+} concentration.

Sample	[Yb^{3+}] (wt%)	τ ($2H_{11/2} \rightarrow 4S_{3/2}$) (μs)	τ ($4I_{13/2}$) (ms)
#1	0	2.5	7.9
#2	0.1	2.5	7.3
#3	0.5	2.5	7.8
#4	1.0	2.3	8.3
#5	2.0	2.5	8.0

concentrations, as it is illustrated in Fig. 4 for sample #4. The experimental lifetime values of $2H_{11/2} \rightarrow 4S_{3/2}$ and $4I_{13/2}$ levels as function of Yb^{3+} concentration are summarized in Table 2. As it can be observed, there is no clear dependency and, in fact, the data seem to indicate that both lifetimes are independent on the ytterbium content.

The situation is completely different in the case of the temporal evolution of the luminescence from the resonant levels, $4I_{11/2}$ (Er^{3+}) and $2F_{5/2}$ (Yb^{3+}), shown in Fig. 5. Although the luminescence decays are complex, and cannot be fitted by a single exponential function, they can be described by using a double exponential function:

$$I(t) = I_1 \exp(-t/\tau_1) + I_2 \exp(-t/\tau_2) \quad (12)$$

where $I(t)$ is the luminescence intensity, t represents the time after the excitation pulse and τ_i ($i = 1, 2$) is the characteristic decay time of the i component with intensity I_i . In this case, it is also usual to characterize the temporal decays given an average decay time ($\langle \tau \rangle$) calculated as:

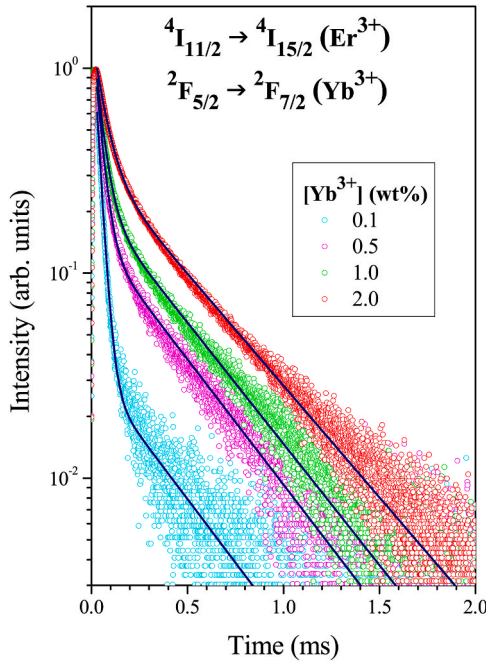


Fig. 5. Temporal evolution, under pulsed excitation at $\lambda_{\text{exc}} = 532$ nm, of the luminescence from the resonant levels $^4I_{11/2} \rightarrow ^4I_{15/2}$ (Er^{3+}) and $^2F_{5/2} \rightarrow ^2F_{7/2}$ (Yb^{3+}) spectrally overlapped transitions).

Table 3

Fitting parameters and average decay time for the luminescence temporal evolution from the resonant levels $^4I_{11/2}$ (Er^{3+}); $^2F_{5/2}$ (Yb^{3+}) as function of Yb^{3+} concentration.

Sample	[Yb ³⁺] (wt%)	I_1 (%)	τ_1 (ms)	I_2 (%)	τ_2 (ms)	$\langle \tau \rangle$ (ms)
#2	0.1	98.2	0.026	1.8	0.350	0.089
#3	0.5	91.1	0.034	8.9	0.355	0.196
#4	1.0	86.3	0.040	13.7	0.367	0.233
#5	2.0	76.5	0.057	23.5	0.398	0.290

$$\langle \tau \rangle = \frac{\int t I(t) dt}{\int I(t) dt} = \frac{I_1^2 \tau_1^2 + I_2^2 \tau_2^2}{I_1 \tau_1 + I_2 \tau_2} \quad (13)$$

The corresponding fitting parameters, I_i and τ_i ($i = 1, 2$), and the average decay time as function of Yb^{3+} concentration are summarized in Table 3.

As it can be seen in Fig. 5, and Table 3, the fast component (τ_1) dominates the decay of the resonant manifolds. In the case of the most diluted sample, $[\text{Yb}^{3+}] = 0.1$ wt%, this time constant ($\tau_1 = 26$ μs) is very close to the reported lifetime value for the $^4I_{11/2}$ erbium manifold [25] ($\tau = 20$ μs), indicating that, in diluted samples, in this temporal scale ($t < 0.2$ ms) the decay is governed by the spontaneous relaxation of $^4I_{11/2}$ erbium level. A detailed inspection of the data reveals that also this fast component suffers a clear lengthening as the Yb^{3+} concentration increases, suggesting that the time needed to activate the transfer processes depends on Yb^{3+} concentration, being lower in samples with high Yb^{3+} content.

At long times the decays are dominated by the slow component (τ_2), which also experience a lengthening as Yb^{3+} concentration increases. In this temporal range the transfer ($\text{Yb}^{3+} \rightarrow \text{Er}^{3+}$) and back transfer processes ($\text{Er}^{3+} \rightarrow \text{Yb}^{3+}$) reach the dynamical equilibrium and the population ratio N_2/N_5 , for a fixed value of Er^{3+} concentration, enhances as Yb^{3+} content increases [26]. As consequence, the decay time tends to higher values since it approaches to the lifetime of the $^2F_{5/2}$ ytterbium excited level.

Table 4

Radiative (A_{ij}) and total ($A_{\text{im}} = 1/\tau_i = A_{ij} + W_{ij}^{\text{NR}}$) transition probabilities.

Transition	Parameter	Value	Reference
$^2H_{11/2}; ^4S_{3/2} \rightarrow ^4F_{9/2}$	A_{76}	3 s^{-1}	[25]
$^2H_{11/2}; ^4S_{3/2} \rightarrow ^4I_{9/2}$	A_{75}	86 s^{-1}	[25]
$^2H_{11/2}; ^4S_{3/2} \rightarrow ^4I_{13/2}$	A_{74}	366 s^{-1}	[25]
$^2H_{11/2}; ^4S_{3/2} \rightarrow ^4I_{15/2}$	A_{73}	1604 s^{-1}	[25]
$^2H_{11/2}; ^4S_{3/2} \rightarrow ^4I_{11/2}$	A_{7m}	$4.0 \times 10^5 \text{ s}^{-1}$	This work
$^4F_{9/2} \rightarrow ^4I_{9/2}, ^4I_{11/2}$	A_{65}	66 s^{-1}	[25]
$^4F_{9/2} \rightarrow ^4I_{13/2}$	A_{64}	67 s^{-1}	[25]
$^4F_{9/2} \rightarrow ^4I_{15/2}$	A_{63}	1225 s^{-1}	[25]
$^4F_{9/2} \rightarrow ^4I_{11/2}$	A_{6m}	$7.0 \times 10^5 \text{ s}^{-1}$	[25]
$^4I_{11/2} \rightarrow ^4I_{13/2}$	A_{54}	28 s^{-1}	[25]
$^4I_{11/2} \rightarrow ^4I_{15/2}$	A_{53}	129 s^{-1}	[25]
$^4I_{11/2} \rightarrow ^4I_{11/2}$	A_{5m}	$5.0 \times 10^4 \text{ s}^{-1}$	[25]
$^4I_{13/2} \rightarrow ^4I_{15/2}$	A_{4m}	125 s^{-1}	This work
$^2F_{5/2} \rightarrow ^2F_{7/2}$	$A_{21} = A_{2m}$	1092 s^{-1}	This work
Cross relaxations			
$^2F_{5/2} \leftrightarrow ^2F_{7/2}$ (Yb^{3+}); $^4I_{15/2} \leftrightarrow ^4I_{11/2}$ (Er^{3+})	$C_{52} = 4.54 \times 10^{-19} + 0.19 \bullet C_{25}$		Eq. (11)
$^2F_{5/2} \rightarrow ^7F_{7/2}$ (Yb^{3+}); $^4I_{11/2} \rightarrow ^4F_{7/2}$ (Er^{3+})	$C_{27} = 1.38 \bullet C_{25}$		Eq. (14)

3.3. Energy transfer modelling: fully determination of the transfer parameters

The energy transfer processes between Er^{3+} and Yb^{3+} ions has been modelled under selective pulsed excitation to the $^4I_{15/2} \rightarrow ^2H_{11/2}$ erbium absorption band in order to compare the simulation results with those presented in the previous section. As it is indicated in Fig. 3, to implement a more realistic model the dominant IR to VIS up-conversion mechanism in $\text{Er}^{3+}/\text{Yb}^{3+}$ co-doped materials was included: the resonant cross relaxation process $^2F_{5/2} \rightarrow ^7F_{7/2}$ (Yb^{3+}); $^4I_{11/2} \rightarrow ^4F_{7/2}$ (Er^{3+}), labelled as C_{27} in figure. For this mechanism, the macroscopic energy transfer parameter can be easily estimated through the erbium electric dipole strengths (A_{ed}) as [5,7]:

$$C_{27} = \frac{A_{\text{ed}}(^4I_{11/2} \rightarrow ^4F_{7/2})}{A_{\text{ed}}(^4I_{15/2} \rightarrow ^4I_{11/2})} C_{25} \approx \frac{134}{97} C_{25} \quad (14)$$

where it has been taken into account the values reported for the transition probabilities of Er^{3+} ions in this glass [25].

The population dynamics under this pulsed pumping scheme can be described by a new set of coupled differential equations:

$$\frac{dN_7}{dt} = R_p N_3 + C_{27} N_2 N_5 - A_{7m} N_7 \quad (15)$$

$$\frac{dN_6}{dt} = (A_{76} + W_{76}^{\text{NR}}) N_7 - A_{6m} N_6 \quad (16)$$

$$\frac{dN_5}{dt} = A_{75} N_7 + (A_{65} + W_{65}^{\text{NR}}) N_6 + C_{25} N_2 N_3 - C_{52} N_5 N_1 - C_{27} N_2 N_5 - A_{5m} N_5 \quad (17)$$

$$\frac{dN_4}{dt} = A_{74} N_7 + A_{64} N_6 + (A_{54} + W_{54}^{\text{NR}}) N_5 - A_{4m} N_4 \quad (18)$$

$$\frac{dN_2}{dt} = C_{52} N_5 N_1 - C_{25} N_2 N_3 - C_{27} N_2 N_5 - A_{2m} N_2 \quad (19)$$

$$N_3 = N_{\text{Er}} - N_4 - N_5 - N_6 - N_7 \quad (20)$$

$$N_1 = N_{\text{Yb}} - N_2 \quad (21)$$

It has been considered that the decay from $^4F_{7/2}$ and $^4I_{9/2}$ levels is completely non radiative to the lower lying levels $^2H_{11/2}$ and $^4I_{11/2}$, respectively. Additionally, the $^2H_{11/2}$ and $^4S_{3/2}$ levels have been treated

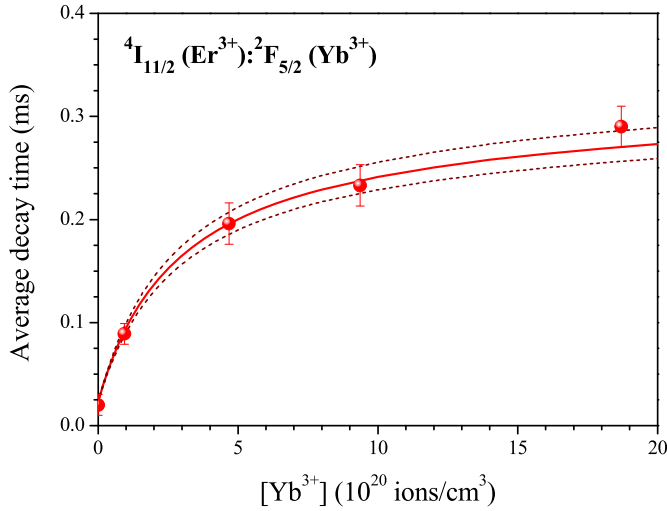


Fig. 6. Average decay time for the resonant levels as function of Yb^{3+} concentration: experimental values (circles) and calculated by numerical integration (lines).

as only one as they are thermally coupled. As it can be observed, eq. (15) contains now the pumping term which was implemented to reproduce the pumping pulse from the Nd:YAG laser used in the experiments (pulse width $t = 10$ ns).

The set of coupled differential equations, eqs. 15–21, have been numerically integrated as function of Yb^{3+} concentration by using a fourth order Runge-Kutta algorithm together with the transition probabilities and transfer parameters shown in Table 4. The total transition probability of the Yb^{3+} excited state in $\text{Ca}_3\text{Al}_2\text{Si}_3\text{O}_{12}$ (A_{2m}) has been determined from the lifetime value ($\tau_2 = 916 \mu\text{s}$) measured in sample #0 ($A_{2m} = 1/\tau_2$, see supplementary information). This procedure allows calculating the population temporal evolution in the different levels, being able to observe not only the decays but also the rise-times induced by the presence of energy transfer processes. It is important to remark that the transfer parameters C_{52} (energy transfer $\text{Er}^{3+} \rightarrow \text{Yb}^{3+}$) and C_{27}

(energy transfer up-conversion) kept linked to the C_{25} value (energy transfer $\text{Yb}^{3+} \rightarrow \text{Er}^{3+}$) through eq. (11) and (14). Therefore, the only fitting parameter used in the numerical integration was the value of C_{25} .

Fig. 6 shows the experimental average decay time (dots) of the resonant $4I_{11/2}(\text{Er}^{3+}): 2F_{5/2}(\text{Yb}^{3+})$ levels (dots) as function of Yb^{3+} concentration. As it can be seen, ytterbium co-doping produces a monotonous increment in the average decay time from the value corresponding to the $4I_{11/2}$ manifold, $\langle \tau \rangle = 20 \mu\text{s}$, in Er^{3+} singly doped samples ($[\text{Yb}^{3+}] = 0$ in figure), up to $\langle \tau \rangle = 290 \mu\text{s}$ when the ytterbium concentration is four times higher than erbium concentration (sample #5).

The experimental data have been fitted using a least square criterion (lines). The best fit was obtained considering a transfer parameter $C_{25} = 5.5 \times 10^{-18} \text{ cm}^3\text{s}^{-1}$, which implies that the back transfer parameter, eq. (11), is $C_{52} = 1.5 \times 10^{-18} \text{ cm}^3\text{s}^{-1}$ and the up-conversion one, eq. (14), is $C_{27} = 7.6 \times 10^{-18} \text{ cm}^3\text{s}^{-1}$ (solid line in Fig. 6). The dashed lines in figure represent the estimated dependencies with $\pm 10\%$ variations in the transfer parameters to take into account the expected uncertainties in the lifetime determination; therefore, they were obtained by integrating eqs. 15–21 considering that $C_{25} = (5.5 \pm 0.5) \times 10^{-18} \text{ cm}^3\text{s}^{-1}$, $C_{52} = (1.5 \pm 0.1) \times 10^{-18} \text{ cm}^3\text{s}^{-1}$ and $C_{27} = (7.6 \pm 0.8) \times 10^{-18} \text{ cm}^3\text{s}^{-1}$.

Fig. 7 shows the experimental temporal evolution of the luminescence (dots) from the main emitting levels recorded in the most diluted sample, $[\text{Yb}^{3+}] = 0.1 \text{ wt\%}$, and in the most concentrated one, $[\text{Yb}^{3+}] = 2.0 \text{ wt\%}$. Figure also includes the luminescent temporal decays calculated by integrating eqs. 15–21 with the transfer parameters C_{25} , C_{52} and C_{27} previously determined (solid lines). As it can be appreciate, there is a good agreement between the luminescence temporal decays experimentally measured and those predicted by the model. In the case of the most concentrated sample, the differences observed in the temporal evolution of the resonant levels, $4I_{11/2}(\text{Er}^{3+})$ and $4F_{5/2}(\text{Yb}^{3+})$, could be related to the apparition of $\text{Yb}^{3+} - \text{Yb}^{3+}$ interactions (basically energy migration, not included in the model) that would produce a lengthening in the luminescent decay.

As a summary, in Fig. 8 the decay times corresponding to the erbium metastable level ($4I_{13/2}$), the resonant levels ($4I_{11/2}(\text{Er}^{3+}): 2F_{5/2}(\text{Yb}^{3+})$) and the thermally coupled manifolds ($2H_{11/2}: 4S_{3/2}$) are depicted as function of Yb^{3+} concentration, where the experimental data (dots) are

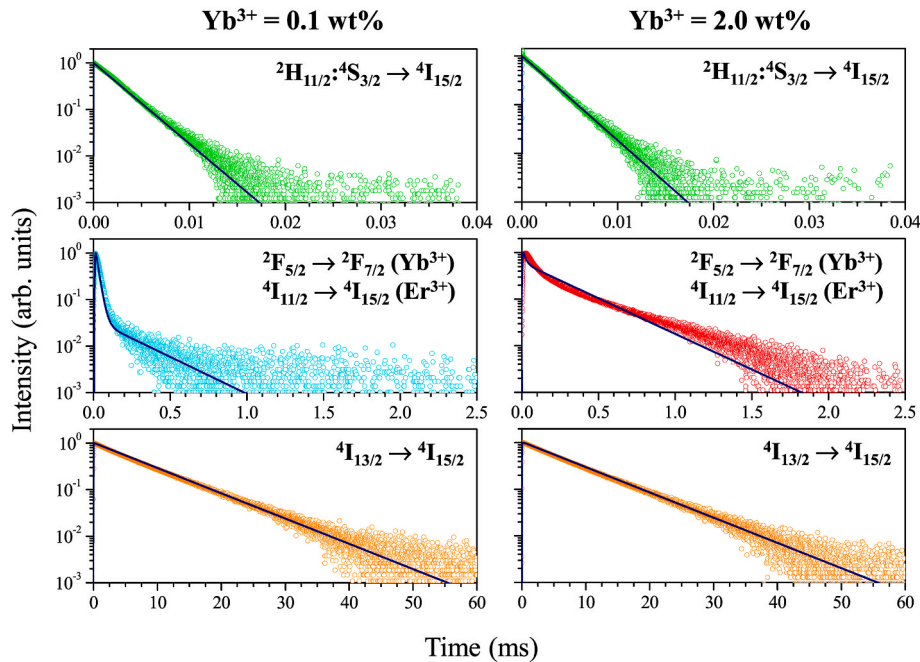


Fig. 7. Comparison between the temporal decays of the main emitting manifolds recorded in samples #2 and #5 (dots) with the predictions obtained by numerical integration (lines) considering that $C_{25} = 5.5 \times 10^{-18} \text{ cm}^3\text{s}^{-1}$.

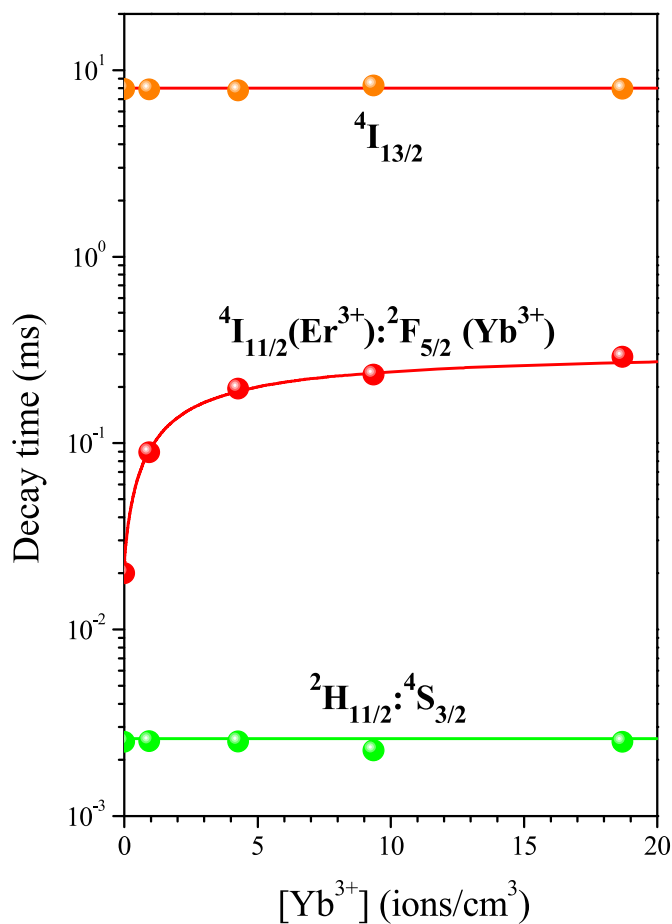


Fig. 8. Experimental and calculated decay times of the main emitting manifolds under pulsed excitation at $\lambda_{\text{exc}} = 532$ nm, dots and solid lines, respectively.

compared with the predictions from the model (solid lines). As it can be seen, in good accordance with the experimental results, the model predicts that under pulsed excitation at $\lambda_{\text{exc}} = 532$ nm the dynamics of the erbium metastable level and the thermally coupled manifolds remain unaltered by the presence of Yb^{3+} ions, even considering the resonant cross relaxation up-conversion mechanism.

4. Conclusions

The macroscopic parameters associated to the resonant cross relaxation processes between Yb^{3+} and Er^{3+} ions in $\text{Ca}_3\text{Al}_2\text{Si}_3\text{O}_{12}$ glasses have been quantified under selective Er^{3+} excitation.

The CW excitation to the $^4\text{I}_{9/2}$ erbium level has been used to access to the main infrared emission bands, which allows to obtain an experimental relationship linking the transfer and back transfer parameters corresponding to the $^2\text{F}_{5/2} \leftrightarrow ^2\text{F}_{7/2}$ (Yb^{3+}): $^4\text{I}_{15/2} \leftrightarrow ^4\text{I}_{11/2}$ (Er^{3+}) cross relaxations.

The dynamics of the main emitting levels has been investigated under pulsed excitation to the $^2\text{H}_{11/2}$ erbium level as function of Yb^{3+} concentration. These measurements, combined with a model based on the rate equations formalism, have allowed the full quantification (absolute values) of the energy transfer parameters. It has been shown that the luminescence temporal evolution of the main emitting levels can be predicted considering that $C_{25} = 5.5 \times 10^{-18} \text{ cm}^3\text{s}^{-1}$, $C_{52} = 1.5 \times 10^{-18} \text{ cm}^3\text{s}^{-1}$ and $C_{27} = 7.6 \times 10^{-18} \text{ cm}^3\text{s}^{-1}$, the last one being estimated from the Judd-Ofelt analysis previously reported.

Finally, it should be remarked that, although the transfer parameters have been determined and checked under selective excitation to Er^{3+}

ions, the obtained values are independent on the excitation scheme. Therefore, they can be used for other purposes such as the understanding of the up-conversion processes under selective Yb^{3+} excitation, or in optimization tasks prior to the development of optical amplifiers and lasers based on $\text{Er}^{3+}/\text{Yb}^{3+}$ co-doped glasses.

Declaration of competing interest

The authors declare that they have no known competing financial interests or personal relationships that could have appeared to influence the work reported in this paper.

Data availability

The data that has been used is confidential.

Acknowledgements

Work partially supported by Ministerio de Ciencia e Innovación (Spain) under project COLUMNAS (PID2019-110632RB-I00). D. Sola acknowledges the PIT2 program of the University of Murcia's own research plan for his financial support.

Appendix A. Supplementary data

Supplementary data to this article can be found online at <https://doi.org/10.1016/j.jlumin.2022.119484>.

References

- [1] C. Cao, W. Qin, J. Zhang, J. Zhang, Y. Wang, Y. Jin, G. Wei, G. Wang, L. Wang, Multicolor up-conversion emissions of $\text{Tm}^{3+}/\text{Er}^{3+}/\text{Yb}^{3+}$ tri-doped YF_3 Phosphors, *J. Nanosci. Nanotechnol.* 8 (2008) 1384–1387.
- [2] P. Moraitis, R.E.I. Schropp, W.G.J.H.M. van Sark, Nanoparticles for luminescent solar concentrators – a review, *Opt. Mater.* 84 (2018) 636–645.
- [3] E. Cantelar, D. Jaque, G. Lifante, Waveguide lasers based on dielectric materials, *Opt. Mater.* 34 (2012) 555–571.
- [4] D.K. Chatterjee, M.K. Gnanasammandhan, Y. Zhang, Small upconverting fluorescent nanoparticles for biomedical applications, *Small* 6 (2010) 2781–2795.
- [5] L.F. Johnson, H.J. Guggenheim, T.C. Rich, F.W. Ostermayer, Infrared-to-visible conversion by rare earth ions in crystals, *J. Appl. Phys.* 43 (1972) 1125–1137.
- [6] Y. Mita, H. Yamamoto, K. Katayanagi, S. Shionoya, Energy transfer processes in Er^{3+} - and Yb^{3+} -doped infrared upconversion materials, *J. Appl. Phys.* 78 (1995) 1219–1223.
- [7] E. Cantelar, J.A. Muñoz, J.A. Sanz-García, F. Cussó, Yb^{3+} to Er^{3+} energy transfer in LiNbO_3 , *J. Phys. Condens. Matter* 10 (1998) 8893–8903.
- [8] M. Marin-Dobrincic, J. García-Sevillano, M. Bettinelli, F. Piccinelli, E. Cantelar, F. Cussó, Quantification of energy transfer processes in $\text{LiLa}_9(\text{SiO}_4)_6\text{O}_2:\text{Er}^{3+}/\text{Yb}^{3+}$ under selective Er^{3+} excitation, *Opt. Express* 22 (2014) 14646–14656.
- [9] A. Polman, F.C.J.M. van Veggel, Broadband sensitizers for erbium-doped planar optical amplifiers: review, *J. Opt. Soc. Am. B* 21 (2004) 871–892.
- [10] G. Karlsson, V. Pasiskevicius, F. Laurell, J.A. Tellefsen, Q-switching of an Er-Yb: glass microchip laser using an acousto-optical modulator, *Opt. Commun.* 217 (2003) 317–324.
- [11] N.A. Tolstik, S.V. Kurilchik, V.E. Kisel, N.V. Kuleshov, V.V. Maltsev, O.V. Pilipenko, E.V. Kaporulina, N.I. Leonyuk, Efficient 1W continuous-wave diode-pumped Er,Yb: $\text{YAl}_3(\text{BO}_3)_4$ laser, *Opt. Lett.* 32 (2007) 3233–3235.
- [12] N.D. Psaila, R.R. Thomson, H.T. Bookey, A.K. Kar, Er, Yb-doped oxyfluoride silicate glass waveguide amplifier fabricated using femtosecond laser inscription, *Appl. Phys. Lett.* 90 (2007), 131102.
- [13] M.C. Stumpf, S.C. Zeller, A. Schlatter, T. Okuno, T. Südmeyer, U. Keller, Compact Er,Yb:glass-laser-based supercontinuum source for high-resolution optical coherence tomography, *Opt. Express* 16 (2008) 10572–10579.
- [14] I. Pavlov, E. Ilbey, E. Dülgergil, A. Bayri, F. Ömer Ilday, High-power high-repetition-rate single-mode Er-Yb-doped fiber laser system, *Opt. Express* 20 (2012) 9471–9475.
- [15] R. Thapa, D. Nguyen, J. Zong, A. Chavez-Pirson, All-fiber fundamentally mode-locked 12 GHz laser oscillator based on an Er/Yb-doped phosphate glass fiber, *Opt. Lett.* 39 (2014) 1418–1421.
- [16] B. Resan, S. Kurmulis, Z.Y. Zhang, A.E.H. Oehler, V. Markovic, M. Mangold, T. Südmeyer, U. Keller, R.A. Hogg, K.J. Weingarten, 10 GHz pulse repetition rate Er:Yb:glass laser modelocked with quantum dot semiconductor saturable absorber mirror, *Appl. Opt.* 55 (2016) 3776–3780.
- [17] T. Sakimura, K. Hirokawa, Y. Watanabe, T. Ando, S. Kameyama, K. Asaka, H. Tanaka, M. Furuta, M. Hagio, Y. Hirano, H. Inokuchi, T. Yanagisawa, 1.55- μm high-peak, high-average-power laser amplifier using an Er,Yb:glass planar

- waveguide for wind sensing coherent Doppler lidar, *Opt Express* 27 (2019) 24175–24187.
- [18] D. Sola, D. Conejos, J.M. de Mendivil, L.O. San Martín, G. Lifante, J.I. Peña, Directional solidification, thermo-mechanical and optical properties of $(\text{Mg}_x\text{Ca}_{1-x})_3\text{Al}_2\text{Si}_3\text{O}_{12}$ glasses doped with Nd^{3+} ions, *Opt Express* 23 (2015) 26356–26368.
- [19] M. Li, Y. Guo, Y. Tian, L. Hu, J. Zhang, 2 μm luminescence and energy transfer characteristic in $\text{Tm}^{3+}/\text{Ho}^{3+}$ co-doped silicate glass, *J. Quantum. Spectrosc. Radiat.* 127 (2013) 70–77.
- [20] D. Dorosz, J. Zmojda, M. Kochanowicz, Investigation on broadband near-infrared emission in $\text{Yb}^{3+}/\text{Ho}^{3+}$ co-doped antimony-silicate glass and optical fiber, *Opt. Mater.* 35 (2013) 2577–2580.
- [21] R. Cao, Y. Lu, Y. Tian, F. Huang, S. Xu, J. Zhang, Spectroscopy of thulium and holmium co-doped silicate glasses, *Opt. Mater. Express* 6 (2016) 2252–2263.
- [22] J. Llorca, V.M. Orera, Directionally-solidified eutectic ceramic oxides, *Prog. Mater. Sci.* 51 (2006) 711–809.
- [23] D. Sola, F.J. Ester, P.B. Oliete, J.I. Peña, Study of the stability of the molten zone and the stresses induced during the growth of $\text{Al}_2\text{O}_3\text{-Y}_3\text{Al}_5\text{O}_{12}$ eutectic composite by the laser floating zone technique, *J. Eur. Ceram. Soc.* 31 (2011) 1211–1218.
- [24] F.J. Ester, D. Sola, J.I. Peña, Thermal stresses in the $\text{Al}_2\text{O}_3\text{-ZrO}_2(\text{Y}_2\text{O}_3)$ eutectic composite during the growth by the laser floating zone technique, *Bol. Soc. Esp. Ceram.* 47 (2008) 352–357.
- [25] G. Lifante, J. Martínez de Mendivil, R. He, E. Cantelar, L. Ortega San Martín, D. Sola, Transition probabilities of Er^{3+} ions in alumino-silicate glasses, *J. Lumin.* 203 (2018) 305–312.
- [26] E. Cantelar, F. Cussó, Analytical solution of the transfer rate equations in $\text{LiNbO}_3\text{:Er}^{3+}/\text{Yb}^{3+}$, *J. Phys. Condens. Matter* 12 (2000) 521–527.